

# A splitting random-choice dynamic relaxation method for smoothed particle hydrodynamics

Yujie Zhu<sup>1</sup>, Chi Zhang<sup>1</sup>, Xiangyu Hu\*

*Department of Mechanical Engineering, Technical University of Munich  
85748 Garching, Germany*

---

## Abstract

For conventional smoothed particle hydrodynamics (SPH), obtaining the static solution of a problem is time-consuming. To address this drawback, we propose an efficient dynamic relaxation method by adding large artificial-viscosity-based damping into the momentum conservation equation. Then, operator splitting methods are introduced to discretize the added viscous term for relaxing the time-step limit. To further improve the convergence rate, a random-choice strategy is adopted, in which the viscous term is imposed randomly rather than at every time step. In addition, to avoid the thread-conflict induced by applying shared-memory parallelization to accelerate implicit method, a splitting cell-linked list scheme is devised. A number of benchmark tests suggest that the present method helps systems achieve equilibrium state efficiently.

*Keywords:* Total Lagrangian SPH, Viscous damping, Dynamic relaxation, Operator splitting

---

\*Corresponding author.

*Email addresses:* [yujie.zhu@tum.de](mailto:yujie.zhu@tum.de) (Yujie Zhu ), [c.zhang@tum.de](mailto:c.zhang@tum.de) (Chi Zhang ), [xiangyu.hu@tum.de](mailto:xiangyu.hu@tum.de) (Xiangyu Hu )

<sup>1</sup>Yujie Zhu and Chi Zhang contributed equally to this work

---

## 1. Introduction

For the numerical simulation of solid dynamic applications undergoing large strain, as an alternative approach to the conventional finite element method (FEM), the meshless methods have attracted more and more interests in recent years [1, 2, 3]. One notable Lagrangian meshless method is smoothed particle hydrodynamics (SPH), which was first introduced by Lucy [4] and Gingold and Monaghan [5] for astrophysics applications. In SPH method, discretization operators are approximated by using the particles within a neighborhood with the help of a weight or smoothing kernel function. This distinct non-local feature makes SPH method can handle large deformations straightforwardly. After its inception, SPH method has been extensively studied and applied to a broad range of problems including fluid dynamics [6, 7, 8, 9], solid dynamics [10, 11, 12], fluid-structure interactions (FSI) [13, 14] and multi-physics applications [15]. In addition, to further improve the numerical accuracy and address the problems of tensile instability and inconsistency [16, 17], many variants of SPH method have been developed. These modifications include the symmetric and normalization formulations [18, 19, 11], the corrective smoothed particle method (CSPH) [20, 21, 22], the finite particle method (FPM) [23, 24] and the stress point algorithm [25, 26, 27]. More applications and their corresponding algorithms can be found in comprehensive reviews as Refs. [3, 28, 29].

Although the accuracy and stability are achieved by SPH methods for the simulation of solid dynamics problems, one has to note that obtaining static solution is very time-consuming because SPH is a typical method with

explicit time-stepping. Therefore, it is necessary to find an efficient method to approximate the converged static or quasi-static displacement. Besides resorting to traditional implicit methods, which solve the entire system with iterative solvers, it is attractive to apply dynamic relaxation, which was proposed for FEM method originally [30, 31, 32], because its explicit iterative algorithm is more efficient for large problems, especially in highly nonlinear cases.

Generally, the dynamic relaxation technique can be classified into two groups, i.e. viscous dynamic relaxation (VDR) and kinetic dynamic relaxation (KDR) [33, 34, 35], according to the manner of applied damping. In VDR, an artificial viscous damping term is added into the equation of motion to accelerate the convergence. One difficulty of VDR is that the solutions for nonlinear problems may be path dependent and vary with different damping ratio as noted in Ref. [36]. Also, the relaxation is slow if insufficient damping ratio is applied, on the other hand, too much damping would also hinder the system from achieving final steady state because the damped velocity can be very small. In KDR, damping is imposed by resetting the velocity to zero at every time step or when kinetic energy reaches maximum. Although the procedure is simple and no damping factor is required, the momentum conservation property is not satisfied in the process of KDR and the convergent rate is not optimal [34, 37].

The main objective of this paper is to propose a dynamic relaxation method, where efficient damping is introduced to SPH for obtaining the static solution. Following VDR, an artificial viscous term is added into the momentum conservation equation to dissipate the velocity gradient of the

system. To address the issue of computational inefficiency when applying explicit scheme to integrate the viscous term, we propose two operator splitting schemes, one is inspired by a method for highly dissipative system [38]. Since such methods treat the viscous term implicitly, they can be unconditional stable and relax the viscous time-step limit, and allow very large damping ratio. To provide a remedy to the issues of path dependency and large damping ratio encountered by the original VDR and KDR, and further accelerate the convergence, we propose a random-choice strategy by which the artificial damping is only carried out at a small fraction of time steps randomly.

For large scale SPH simulations, two parallelization strategies, viz. shared and distributed memories, are implemented for accelerating computational performance. For shared memory parallelization strategy, thread-conflict occurs when implicit scheme is applied. To address this issue, a thread-safe splitting cell-linked list (CLL) scheme is proposed for implementing shared memory parallelization to accelerate implicit scheme. In our code, the open-source Threading Building Blocks (TBB) library [39] developed by INTEL is applied for providing the share-memory parallel programming environment.

The remainder of this paper is organized as follows. Section 2 briefly reviews the governing equations and total Lagrangian SPH (TLSPH) formulations for solid dynamics. The details of the present artificial damping method and the splitting CLL scheme are described in Section 3. Numerical examples are presented and discussed in Section 4 and then concluding remarks are given in Section 5. The corresponding code of this work are available on GitHub at <https://github.com/Xiangyu-Hu/SPHinXsys> [40].

## 2. Preliminary

### 2.1. Total Lagrangian solid dynamics

In total Lagrangian formalism, the conservation of mass and momentum for solid dynamics can be expressed as

$$\begin{cases} \rho = \rho^0 J^{-1} \\ \rho^0 \frac{d\mathbf{v}}{dt} = \nabla^0 \cdot \mathbb{P}^T + \rho^0 \mathbf{g} \end{cases}, \quad (1)$$

where  $\rho$  is the density, Jacobian  $J = \det(\mathbb{F})$ ,  $\mathbf{v}$  the velocity,  $\mathbf{g}$  body-force and  $\mathbb{P}$  the first Piola-Kirchhoff stress tensor.  $\mathbb{F}$  is the deformation gradient and is defined as

$$\mathbb{F} = \nabla^0 \mathbf{u} + \mathbb{I}, \quad (2)$$

where  $\mathbb{I}$  denotes the identity matrix and  $\mathbf{u}$  the displacement vector. Note that the superscript  $(\cdot)^0$  denotes the quantities in the reference configuration thereafter. For ideal elastic or Kirchhoff material, the first Piola-Kirchhoff stress tensor  $\mathbb{P}$ , can be evaluated by

$$\mathbb{P} = \mathbb{F}\mathbb{S}. \quad (3)$$

Here,  $\mathbb{S}$  denotes the second Piola-Kirchhoff stress tensor and it can be evaluated via constitutive equation. In particular, for isotropic and linear elastic materials, the constitutive equation can be simplified to

$$\begin{aligned} \mathbb{S} &= K \text{tr}(\mathbb{E}) \mathbb{I} + 2G \left( \mathbb{E} - \frac{1}{3} \text{tr}(\mathbb{E}) \mathbb{I} \right) \\ &= \lambda \text{tr}(\mathbb{E}) \mathbb{I} + 2\mu \mathbb{E}, \end{aligned} \quad (4)$$

where  $\lambda$  and  $\mu$  are Lamé coefficients and  $\mathbb{E}$  represents the Green-Lagrangian strain tensor defined by

$$\mathbb{E} = \frac{1}{2} (\mathbb{F}^T \mathbb{F} - \mathbb{I}). \quad (5)$$

Also,  $K = \lambda + 2\mu/3$  and  $G = \mu$  denote the bulk and the shear modulus, respectively. They have the following relationship

$$E = 2G(1 + 2\nu) = 3K(1 - 2\nu), \quad (6)$$

with  $E$  representing the Young's modulus and  $\nu$  the Poisson's ratio. In this work, the neo-Hookean material with the strain energy density function

$$\mathcal{W} = \mu \text{tr}(\mathbb{E}) - \mu \ln J + \frac{\lambda}{2} (\ln J)^2 \quad (7)$$

is also considered to predict the nonlinear stress-strain behavior of materials undergoing large deformations. The corresponding second Piola-Kirchhoff stress  $\mathbb{S}$  can be evaluated by

$$\mathbb{S} = \frac{\partial \mathcal{W}}{\partial \mathbb{E}}. \quad (8)$$

## 2.2. Total Lagrangian SPH method

In TLSPH method, the kernel correction matrix  $\mathbb{B}^0$  is defined as [41]

$$\mathbb{B}_i^0 = \left( - \sum_j^N V_j^0 \mathbf{r}_{ij}^0 \otimes \nabla_i^0 W_{ij} \right)^{-1}, \quad (9)$$

where  $\mathbf{r}_{ij}^0 = \mathbf{r}_i^0 - \mathbf{r}_j^0$  and

$$\nabla_i^0 W_{ij} = \left( \frac{\partial W_{ij}}{\partial r_{ij}} \right)^0 \mathbf{e}_{ij} \quad (10)$$

represents the gradient of the kernel function calculated at the initial reference configuration and  $V_j^0$  denotes the particle volume. Here,  $\mathbf{e}_{ij}^0 = \frac{\mathbf{r}_{ij}^0}{|\mathbf{r}_{ij}^0|}$ . According to the equation of mass conservation Eq. (1), the density can be evaluated directly as

$$\rho_i = \rho_i^0 J^{-1}. \quad (11)$$

Then, the equation of momentum conservation in Eq. (1) is discretized as

$$\frac{d\mathbf{v}_i}{dt} = \frac{2}{m_i} \sum_j^N V_i^0 V_j^0 \tilde{\mathbb{P}}_{ij} \nabla_i^0 W_{ij} + \mathbf{g}, \quad (12)$$

where

$$\tilde{\mathbb{P}}_{ij} = \frac{1}{2} (\mathbb{P}_i \mathbb{B}_i^0 + \mathbb{P}_j \mathbb{B}_j^0) \quad (13)$$

denotes the inter-particle averaged first Piola-Kirchhoff stress and  $m_i$  is the particle mass. Here, the first Piola-Kirchhoff stress tensor is computed with the constitutive law where the deformation tensor  $\mathbb{F}$  is updated by

$$\frac{d\mathbb{F}_i}{dt} = - \left( \sum_j V_j^0 \mathbf{v}_{ij} \otimes \nabla_i^0 W_{ij} \right) \mathbb{B}_i^0, \quad (14)$$

with  $\mathbf{v}_{ij} = \mathbf{v}_i - \mathbf{v}_j$  the relative velocity between particle  $i$  and  $j$ .

### 2.3. Time integration

Following the work of Zhang et al. [14], the position-based Verlet scheme is adopted for time integration. First, update the deformation tensor, density and particles position to a midpoint stage as

$$\begin{cases} \mathbb{F}_i^{n+\frac{1}{2}} = \mathbb{F}_i^n + \frac{1}{2} \Delta t \left( \frac{d\mathbb{F}_i}{dt} \right)^n \\ \rho_i^{n+\frac{1}{2}} = \rho_i^0 (J_i^n)^{-1} \\ \mathbf{r}_i^{n+\frac{1}{2}} = \mathbf{r}_i^n + \frac{1}{2} \Delta t \mathbf{v}_i^n \end{cases} . \quad (15)$$

Then, particles velocity at new time step is update by

$$\mathbf{v}_i^{n+1} = \mathbf{v}_i^n + \Delta t \left( \frac{d\mathbf{v}_i}{dt} \right)^n . \quad (16)$$

Finally, the deformation tensor, density as well as positions of particles at the new stage are evaluated by

$$\begin{cases} \mathbb{F}_i^{n+1} = \mathbb{F}_i^{n+\frac{1}{2}} + \frac{1}{2}\Delta t \left(\frac{d\mathbb{F}_i}{dt}\right)^{n+\frac{1}{2}} \\ \rho_i^{n+1} = \rho_i^0 \left(J_i^{n+\frac{1}{2}}\right)^{-1} \\ \mathbf{r}_i^{n+1} = \mathbf{r}_i^{n+\frac{1}{2}} + \frac{1}{2}\Delta t \mathbf{v}_i^{n+\frac{1}{2}} \end{cases} . \quad (17)$$

For numerical stability, the acoustic and body-force time-step criterion are considered, i.e.

$$\Delta t = 0.6 \min \left( \frac{h}{c + |\mathbf{v}|_{max}}, \sqrt{\frac{h}{\left|\frac{d\mathbf{v}}{dt}\right|_{max}}} \right), \quad (18)$$

where  $h$  denotes the smoothing length and  $c$  is the sound speed of solid structure given by  $c = \sqrt{K/\rho}$ .

### 3. Dynamic relaxation method

To damp the velocity gradient of a system, an artificial viscous force can be introduced into the momentum conservation equation Eq. (1). Subsequently, the momentum conservation equation for solid dynamics can be rewritten as

$$\rho^0 \frac{d\mathbf{v}}{dt} = \nabla^0 \cdot \mathbb{P}^T + \rho^0 \mathbf{g} + \eta (\nabla^0)^2 \mathbf{v}, \quad (19)$$

where  $\eta = \rho^0 \nu$  denotes the artificial dynamic viscosity. Following the total Lagrangian formulation, the viscous damping term can be discretized as

$$\left(\frac{d\mathbf{v}_i}{dt}\right)^\nu = \eta (\nabla^0)^2 \mathbf{v} = \frac{2\eta}{m_i} \sum_j^N V_i^0 V_j^0 \frac{\mathbf{v}_{ij}}{r_{ij}} \left(\frac{\partial W_{ij}}{\partial r_{ij}}\right)^0. \quad (20)$$



Note that if the added damping term is solved by an explicit scheme, the time-step size, along with the acoustic and body-force time-step size criterion of Eq. (18), would be also constrained by

$$\Delta t \leq 0.5 \frac{h^2}{\nu D}, \quad (21)$$

where  $D = \{1, 2, 3\}$  for one-, two- or three-dimensional cases, respectively. To achieve fast convergence, a suitable large damping ratio is preferred. Therefore, the overall time-step size may be limited by the above viscous criteria, in particular when high spatial resolution is applied, and this leads to excessive computational efforts.

In this work, we first apply an operator splitting method following Ref. [42] to decouple the momentum conservation equation Eq.(19) into two procedures, i.e. the original momentum part

$$S_m \quad : \quad \rho^0 \frac{d\mathbf{v}}{dt} = \nabla^0 \cdot \mathbb{P}^T + \rho^0 \mathbf{g}, \quad (22)$$

and the damping part

$$S_d \quad : \quad \frac{d\mathbf{v}}{dt} = \eta (\nabla^0)^2 \mathbf{v}. \quad (23)$$

Here, two operators  $S_m$  and  $S_d$  are introduced to represent the original momentum equation without viscosity and the damping process, respectively. Subsequently, the first order accuracy Lie-Trotter splitting scheme [43] is applied to approximate the solution from time  $t$  to  $t + \Delta t$  by

$$\mathbf{v}(t + \Delta t) = S_d^{(\Delta t)} \circ S_m^{(\Delta t)} \mathbf{v}(t), \quad (24)$$

where the symbol  $\circ$  denotes the separation of each operator and indicates that  $S_d^{(\Delta t)}$  is applied after  $S_m^{(\Delta t)}$ . If implicit methods are adopted to discretize the

viscous term, the damping step can be unconditionally stable and thus a larger time-step size is allowed.

One should note that large scale matrix operations or iterations over the entire system for traditional implicit methods lead to large memory requirement and difficulties in parallelization. To avoid this problem, we continue to split the entire-domain-related damping step into particle-by-particle operators, e.g. by second-order Strang splitting [44], as

$$S_d^{(\Delta t)} = D_1^{(\frac{\Delta t}{2})} \circ D_2^{(\frac{\Delta t}{2})} \circ \dots \circ D_{N_t-1}^{(\frac{\Delta t}{2})} \circ D_{N_t}^{(\frac{\Delta t}{2})} \circ D_{N_t}^{(\frac{\Delta t}{2})} \circ D_{N_t-1}^{(\frac{\Delta t}{2})} \circ \dots \circ D_2^{(\frac{\Delta t}{2})} \circ D_1^{(\frac{\Delta t}{2})}, \quad (25)$$

where  $N_t$  denotes the total number of particles and  $D_i$  the split damping operator corresponding to particle  $i$ . In the following, we propose two efficient schemes to the local damping operator, where velocities are updated implicitly and locally. Then, the new time-step velocity updating for the entire field can be achieved by carrying out the local split operator to all particles for half a time step and then backwards for another half time step [45] as shown in Eq.(25).

### 3.1. Particle-by-particle splitting scheme

In an implicit formulation, the local damping term in Eq. (20) can be rewritten as

$$\left(\frac{d\mathbf{v}_i}{dt}\right)^\nu = \frac{2\eta}{m_i} \sum_j^N V_i^0 V_j^0 \frac{\mathbf{v}_{ij}^{n+1}}{r_{ij}} \left(\frac{\partial W_{ij}}{\partial r_{ij}}\right)^0 \quad (26)$$

with  $\mathbf{v}_{ij}^{n+1} = \mathbf{v}_{ij}^n + d\mathbf{v}_i - d\mathbf{v}_j$ . We denote

$$B_j = 2\eta V_i^0 V_j^0 \frac{1}{r_{ij}} \left(\frac{\partial W_{ij}}{\partial r_{ij}}\right)^0 dt \quad (27)$$

and

$$\mathbf{E}_i = -2\eta \sum_j^N V_i^0 V_j^0 \frac{\mathbf{v}_{ij}^n}{r_{ij}} \left( \frac{\partial W_{ij}}{\partial r_{ij}} \right)^0 dt = - \sum_j^N B_j \mathbf{v}_{ij}^n. \quad (28)$$

The implicit formulation Eq.(26) can be further transformed as

$$\mathbf{E}_i = \left( \sum_j^N B_j - m_i \right) d\mathbf{v}_i - \sum_j^N B_j d\mathbf{v}_j, \quad (29)$$

where  $d\mathbf{v}_i$  and  $d\mathbf{v}_j$  represent the incremental change for velocity of particle  $i$  and its neighboring particles  $j$  induced by viscous acceleration. Here, we adopt the gradient descent method [46] to evaluate  $d\mathbf{v}_i$  and  $d\mathbf{v}_j$ . Specifically, the left hand side (LHS) of Eq. (29) can be decreased by following its gradient. With respect to variables  $(d\mathbf{v}_i, d\mathbf{v}_1, d\mathbf{v}_2, \dots, d\mathbf{v}_N)^T$ , the gradient  $\nabla \mathbf{E}_i$  gives

$$\nabla \mathbf{E}_i = \left( \sum_j^N B_j - m_i, -B_1, -B_2, \dots, -B_N \right)^T. \quad (30)$$

We choose

$$(d\mathbf{v}_i, d\mathbf{v}_1, d\mathbf{v}_2, \dots, d\mathbf{v}_N)^T = \mathbf{k} \nabla \mathbf{E}_i, \quad (31)$$

where  $\mathbf{k}$  is known as the learning rate [46]. By substituting Eqs. (30) and (31) into Eq. (29), the learning rate can be obtained, i.e.

$$\mathbf{k} = \left( \left( \sum_j^N B_j - m_i \right)^2 + \sum_j^N (B_j)^2 \right)^{-1} \mathbf{E}_i. \quad (32)$$

According to Eqs. (30) and (31), the incremental change for velocity by viscous damping can be thus achieved. In order to ensure momentum conservation, the velocities of neighboring particles are then modified by the above predicted incremental change. In summary, the local update of velocities includes two steps as follows. The first step calculates the incremental

change for velocity by gradient descent method, i.e.

$$\begin{cases} \mathbf{v}_i^{n+1} &= \mathbf{v}_i^n + d\mathbf{v}_i = \mathbf{v}_i^n + \left(\sum_j^N B_j - m_i\right) \mathbf{k} \\ \mathbf{v}_1^p &= \mathbf{v}_1^n + d\mathbf{v}_1 = \mathbf{v}_1^n - B_1 \mathbf{k} \\ \mathbf{v}_2^p &= \mathbf{v}_2^n + d\mathbf{v}_2 = \mathbf{v}_2^n - B_2 \mathbf{k} \\ &\dots \\ \mathbf{v}_N^p &= \mathbf{v}_N^n + d\mathbf{v}_N = \mathbf{v}_N^n - B_N \mathbf{k} \end{cases}, \quad (33)$$

where the superscript  $p$  denotes the predicted value. The second step ensures momentum conservation, which yields

$$\begin{cases} \mathbf{v}_1^{n+1} &= \mathbf{v}_1^n - B_1 (\mathbf{v}_i^{n+1} - \mathbf{v}_1^p) / m_1 \\ \mathbf{v}_2^{n+1} &= \mathbf{v}_2^n - B_2 (\mathbf{v}_i^{n+1} - \mathbf{v}_2^p) / m_2 \\ &\dots \\ \mathbf{v}_N^{n+1} &= \mathbf{v}_N^n - B_N (\mathbf{v}_i^{n+1} - \mathbf{v}_N^p) / m_N \end{cases}. \quad (34)$$

As the velocities are updated implicitly and much larger time-step size is allowed. In this work, we choose the following viscous criterion

$$\Delta t \leq 50 \frac{h^2}{\nu D}. \quad (35)$$

Note that this criterion is about 100 times larger than the corresponding explicit method as presented in Eq. (21). Besides, the artificial dynamic viscosity  $\eta = \rho^0 \nu$  as shown in Eq. (19) is defined by

$$\eta = \frac{1}{4} \beta \rho^0 \sqrt{\frac{E}{\rho}} L = \frac{\beta}{4} \sqrt{\rho^0 E} L, \quad (36)$$

where  $L$  is the characteristic length scale of the problem and  $\beta$  denotes a parameter relating to the body shape. Note that choose different value for the parameter  $\beta$  may variate, though not much, the convergence rate.

### 3.2. Pairwise splitting scheme

Inspired by the work of Ref. [38], we present herein the pairwise splitting scheme where particle velocity is updated implicitly and locally in a pairwise fashion. By adopting the second-order Strang splitting [44], the damping operator corresponding to each particle  $i$  as given in Eq. (25) is further split based on its neighbors, i.e.

$$D_i^{(\Delta t)} = D_{i,1}^{(\frac{\Delta t}{2})} \circ D_{i,2}^{(\frac{\Delta t}{2})} \circ \cdots \circ D_{i,N-1}^{(\frac{\Delta t}{2})} \circ D_{i,N}^{(\frac{\Delta t}{2})} \circ D_{i,N}^{(\frac{\Delta t}{2})} \circ D_{i,N-1}^{(\frac{\Delta t}{2})} \circ \cdots \circ D_{i,2}^{(\frac{\Delta t}{2})} \circ D_{i,1}^{(\frac{\Delta t}{2})}, \quad (37)$$

where  $D_{i,j}^{(\frac{\Delta t}{2})}$  denotes the interaction between particle  $i$  and its neighbors. Specifically, the incremental changes for velocity of a specific particle pair induced by viscosity can be written in implicit form as

$$\begin{cases} m_i d\mathbf{v}_i = B_j (\mathbf{v}_{ij} + d\mathbf{v}_i - d\mathbf{v}_j) \\ m_j d\mathbf{v}_j = -B_j (\mathbf{v}_{ij} + d\mathbf{v}_i - d\mathbf{v}_j) \end{cases}. \quad (38)$$

Here,  $B_j$  is defined in Eq. (27) and it is obvious that this process does not change the conservation of momentum. Then,  $d\mathbf{v}_i$  and  $d\mathbf{v}_j$  can be obtained straightforwardly by solving Eq. (38), which yields

$$\begin{cases} d\mathbf{v}_i = m_j \frac{B_j \mathbf{v}_{ij}}{m_i m_j - (m_i + m_j) B_j} \\ d\mathbf{v}_j = -m_i \frac{B_j \mathbf{v}_{ij}}{m_i m_j - (m_i + m_j) B_j} \end{cases}. \quad (39)$$

By sweeping over all neighboring particle pairs for half a time step and then backwards for another half time step, the incremental changes for velocity of particle  $i$  and all its neighbors can be thus achieved. Compared to the particle-by-particle splitting method in Section 3.1, this scheme leads more errors in solving viscosity due to the further splitting in pairwise fashion.

However, it is unconditional stable and thus more suitable for problems with high spatial resolution and high damping ratio.

### 3.3. Random-choice strategy

As noted in Ref.[36], the solutions for nonlinear problems are path dependent and may vary with different damping ratio. The added viscous force would hinder the system achieving correct static state especially when the damping ratio is large. Thus, a suitable damping ratio has to be selected [36, 47] for faster convergence of the system with the aforementioned viscous damping methods.

To avoid this problem and relax the limitation on the choice of large damping ratio, we present herein a random-choice strategy in which the viscosity term is imposed randomly rather than at every time step. For this, the artificial dynamic viscosity  $\eta$  is modified as

$$\tilde{\eta} = \begin{cases} \eta/\alpha & \text{if } \alpha < \phi \\ 0 & \text{otherswise} \end{cases}, \quad (40)$$

where  $\phi$  is a random number uniformly distributed between 0 to 1.  $\alpha$  is a parameter determining the probability, and we set  $\alpha = 0.2$  in this work. Therefore, the resistance on displacement induced by the large artificial viscosity can be released randomly, as will shown the numerical example (Section 4.1), which eliminates the path dependency and accelerates the convergence. Note that this strategy also helps to save much of computational cost since the computation of damping is only carried out at a small fraction of time steps.

### 3.4. *Splitting cell-linked list*

Shared-memory parallel technique is widely used in SPH simulation due to its easy-implementation nature. However, for the above two proposed implicit approaches, implementing shared-memory approach taking advantage of multicore performance, is problematic. Since the velocities of particle  $i$  and the neighbors are updated simultaneously in above implicit method, conflicts may happen when the values of one particle pair are updated at the same time by multiple threads.

In order to avoid this problem, a splitting CLL method is proposed. Figure 1 presents a sketch of the splitting CLL method in two-dimensional space. Similar to the conventional CLL method, the computational domain is divided into cells with the same size to reduce the searching space [48] and the cell spacing  $r_c$  is equal to the cut-off radius of the kernel function. Then, the cell domain is divided into 9 blocks (27 blocks for three-dimensional space) and all the cells are assigned to blocks. To implement the share-memory parallelization between blocks, each block satisfies the condition that all its cells are not neighboring cells to each other. As shown in Figure 1, cells are assigned to block 1 with condition of  $(\text{Cell}_i \subset \text{Block1} | \{i = 1, 4, 7, 28, 31, 34\})$  and also cells are assigned to block 9 with condition of  $(\text{Cell}_i \subset \text{Block9} | \{i = 21, 24, 27, 48, 51, 54\})$ . When the tasks are distributed to threads based on blocks, the particles executed by different threads are at least two cell space away from each other at any time. The conflicts can be thus avoid, since the neighboring particles only locate in the same cell or other adjacent 8 cells.

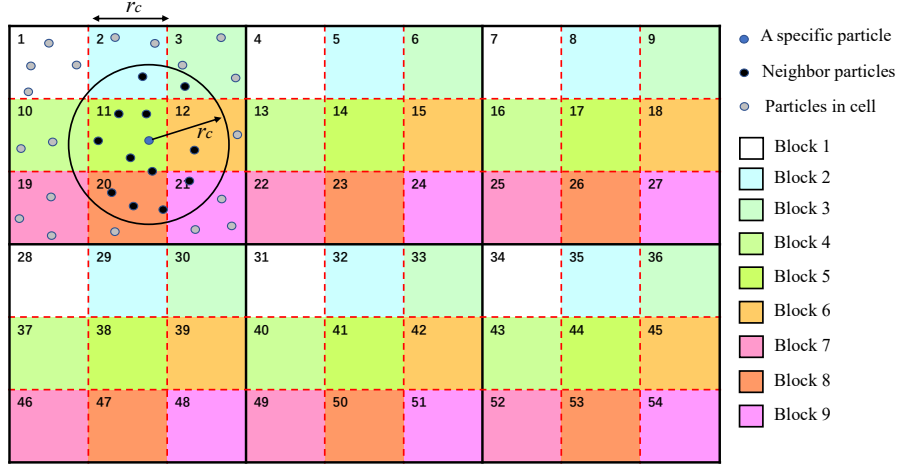


**Figure 1:** Sketch of the splitting CLL method in two-dimensional space.

## 4. Numerical examples

In this section, various tests for static equilibrium simulation including cantilever bending and twisting, ball free falling and a fluid-structure interaction problem are simulated to demonstrate the effectiveness and efficiency of the present method. In the following cases, the 5th-order C2 Wendland kernel [49] is adopted and the smoothing length  $h = 1.3dp$  with  $dp$  denoting the initial particle spacing. Term "No damping" denotes the conventional TLSPH method without damping imposed, term "Reference" is the static solution obtained by the conventional TLSPH method and term "Present" represents the particle-by-particle splitting damping method presented in Section 3.1 if not mentioned otherwise.

### 4.1. Bending cantilever

We first consider a three dimensional cantilever bending under gravity. As shown in Figure 2, one end of the cantilever is clamped to the wall and



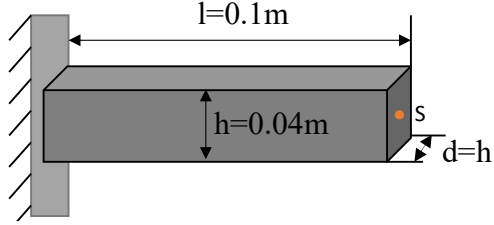
the body bends freely under the gravity  $g = 9.8m/s^2$ . The neo-Hookean material with density  $\rho = 1265kg/m^3$ , Young's modulus  $E = 5 \times 10^4Pa$  and Poisson's ratio  $\nu = 0.45$  is applied. This case is studied with three different spatial resolutions, i.e.  $h/dp = \{6, 12, 24\}$ . The artificial viscosity  $\eta_0 = \frac{\beta}{4}\sqrt{\rho E}d = 32kg/(m \cdot s)$  with  $\beta = d/l = 0.4$  is applied.

Figure 3 presents the deformed configuration in equilibrium state with three different spatial resolutions. The time histories of the displacement in  $y$ -direction of the point  $S$  are given in Figure 4. It is clear that the conventional TLSPH method exhibits oscillations and takes long time to reach the steady state. As for the present method, only a few oscillations are exhibited and the steady state is reached quickly which reduces much computational time for static solution. Besides, with the conventional TLSPH method, the final displacements of point  $S$  in  $y$ -direction with  $h/dp = 6$ ,  $h/dp = 12$  and  $h/dp = 24$  are  $-9.90 \times 10^{-3}m$ ,  $-6.89 \times 10^{-3}m$  and  $-5.86 \times 10^{-3}m$ , respectively. We can observe that the same static results are obtained by the present method and a converge solution is achieved with increasing resolutions.

To test the performance of the adopted random-choice strategy, the setup with parameter  $\alpha = 1$  of Eq. (40) and artificial viscosity  $\eta = 5\eta_0$  and  $\eta = 10\eta_0$  are also considered. The top panel of Figure 5 shows the comparison of the present method with different parameters at the resolution of  $h/dp = 12$ . We can observe that the results of  $\alpha = 1$ , in which the viscous damping is imposed at every time-step, cannot achieve the final state even at  $t = 1.5s$  especially for higher artificial viscosity. Also note that lager damping leads larger distance between the solution to that of the final state and the velocity approaching to final state becomes very small due to too much damping.

However, with the help of the random-choice strategy, e.g.  $\alpha = 0.2$ , the system is released randomly from large damping and the same final state can be reached efficiently for both  $\eta = 5\eta_0$  and  $\eta = 10\eta_0$ . Besides, the pairwise splitting scheme as presented in Section 3.2 is also introduced to discretize the viscous term in this case. The bottom panel of Figure 5 gives the corresponding results with different parameters at the resolution of  $h/dp = 12$ . Compared to that of the top panel, it can be observed that the viscosity achieved by the pairwise splitting scheme is less than the splitting scheme presented in Section 3.1. However, with higher artificial viscosity, the steady state of the cantilever can also be achieved efficiently. Meanwhile, this pairwise splitting scheme is more stable and free from the limitation of viscous criterion, which is more suitable for the problem with high resolution and high damping ratio.

The computational performance of the present method by implementing the shared-memory parallelization and random-choice strategies is then tested. The computation is conducted with spatial resolution of  $h/dp = 12$  and the total physical time of  $t = 2s$  on an AMD Ryzen 5 3600 6-Core CPU Desktop computer with 16GB RAM and Windows system (10). Table 1 reports the CPU wall-clock time for the process of viscous damping. We can see that the shared-memory parallelization strategy demonstrates about 2.8 speedup compared to that of serial computing. Besides, the random-choice strategy also saves much computational efforts and only takes 20% ( $\alpha = 0.2$ ) CPU time compared to the one without applying this strategy. The viscous damping process only takes 2.38s during the whole computation and optimized computational performance is achieved.



**Figure 2:** Bending cantilever: Initial configuration. Probe  $S$  is located at the free-end of the cantilever.

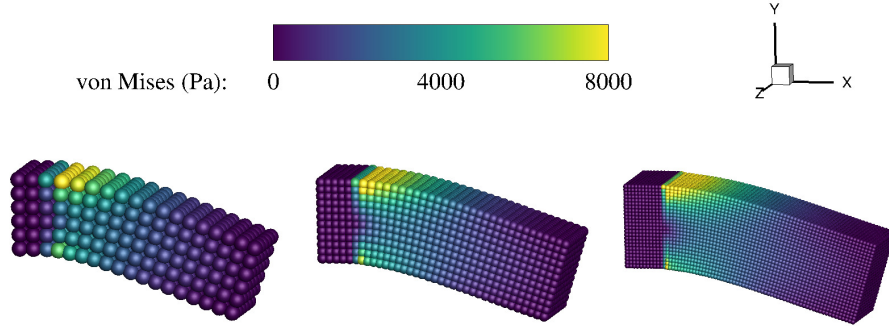


**Figure 3:** Bending cantilever: Deformed configuration in steady state at resolution of  $h/dp = 6$  (left panel),  $h/dp = 12$  (middle panel) and  $h/dp = 24$  (right panel).

#### 4.2. Twisting cantilever

Under a rotational body-force, the cantilever as presented in Section 4.1 can be twisted from the initial configuration. As shown in Figure 6, the bottom of the cantilever is also clamped and a sinusoidal rotational body-force is imposed. The body-force relates to the origin and is defined by

$$g = [0, y\gamma, z\gamma]^T, \quad (41)$$

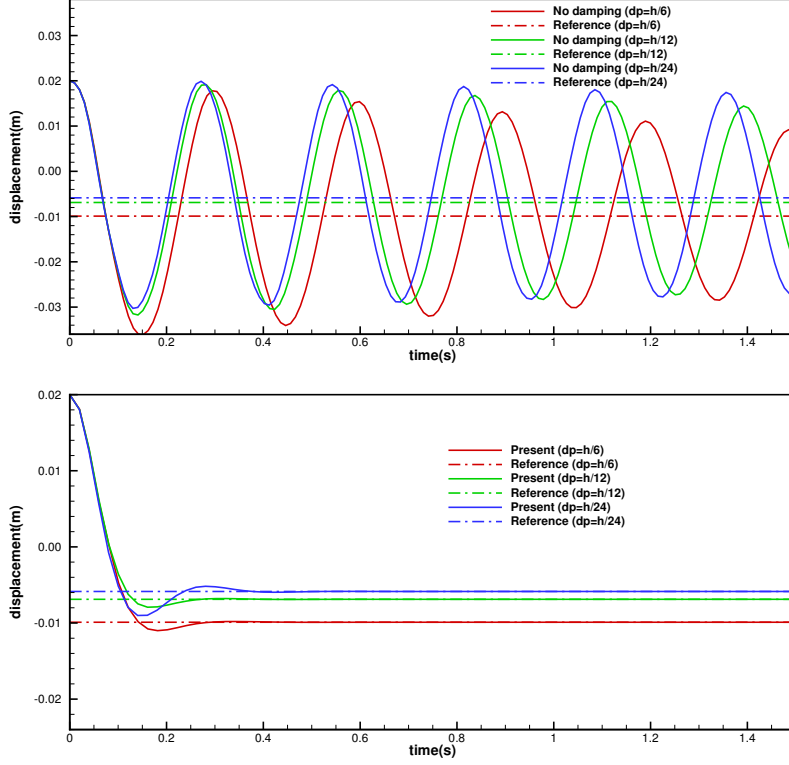


**Figure 4:** Bending cantilever: The time history displacement of the end point  $S$  in vertical direction obtained by conventional method (top panel) and the present method (bottom panel).

where  $\gamma = \frac{20g}{h} \sin(\pi x/2L)$  and  $g = 9.8m/s^2$ . The similar neo-Hookean material property as in bending case is adopted and this case is performed at the resolution of  $h/dp = 12$ .

Figure 7 and 8 present several snapshots of the deformation and the time history displacement in  $z$ -direction of the point  $S$ , respectively. With the present viscous damping imposed, the final steady state of the system is reached much faster and the same result with that of the conventional TLSPH

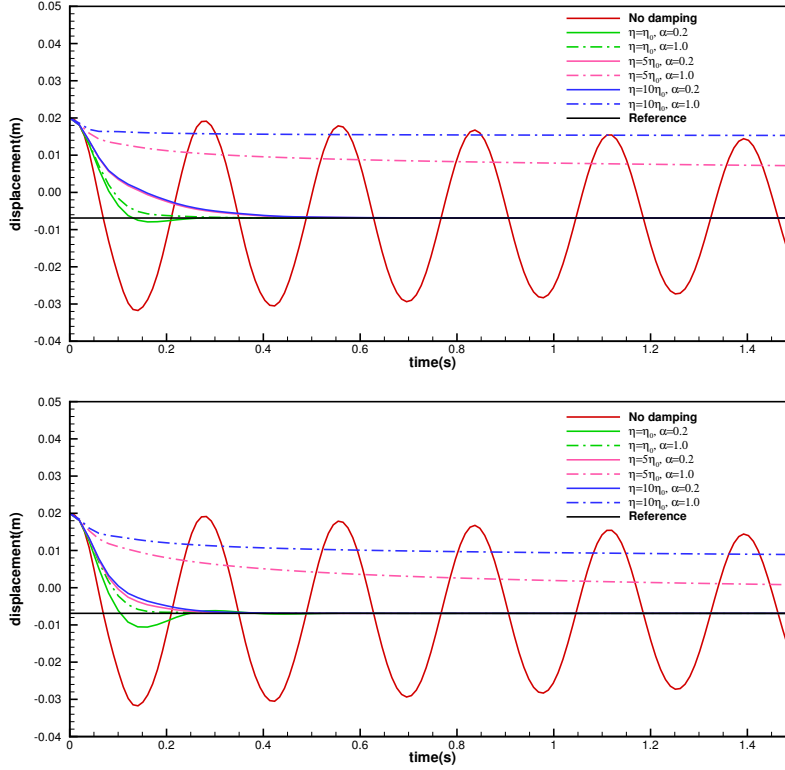


**Figure 5:** Bending cantilever: Comparisons of the time history displacement of point  $S$  at the resolution of  $h/dp = 12$  by the operator splitting method (top panel) and the pairwise splitting method (bottom panel).

is achieved implying the efficiency and accuracy of the present method.

#### 4.3. Ball free falling

A two dimensional ball free falling is considered herein. Figure 9 gives the initial configuration and the body-fitted particle distribution of the ball. In this case, a ball falls freely accelerated by gravity  $g = 9.8m/s^2$  and collides with the floor. A linear elastic material with density  $\rho = 1000kg/m^3$ , Young's modulus  $E = 5 \times 10^5 Pa$  and Poisson's ratio  $\nu = 0.45$  is adopted and the

**Table 1:** CPU time for viscous damping process in the simulation of Bending cantilever with different parameters.

CPU time (s)	serial computation	parallel computation
$\alpha = 1.0$	32.82	11.61
$\alpha = 0.2$	6.66	2.38

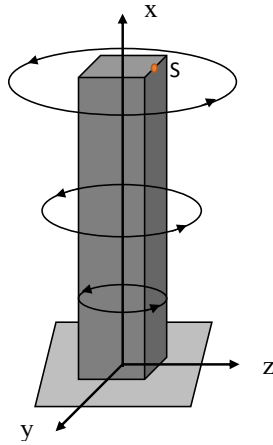


**Figure 6:** Twisting cantilever: Initial configuration. Probe  $S$  locates at the free-end of the cantilever.

initial particle spacing  $dp = 0.02d$ . For the present method, the artificial viscosity is given by  $\eta = \frac{\beta}{4}\sqrt{\rho E}d = 5590kg/(m \cdot s)$  with  $\beta = 1$ .

Figure 10 shows four snapshots of the ball deformation and the corresponding von Mises stress. After several collisions, the equilibrium of this system is reached and the ball stands still on the wall. Figure 11 gives the time history of the displacement of the ball center in vertical direction. It is obvious that achieving steady state of the system for the conventional TLSPH method is time-consuming and more collisions are exhibited in the simulation. The amplitude reduction is mainly caused by the numerical dissi-

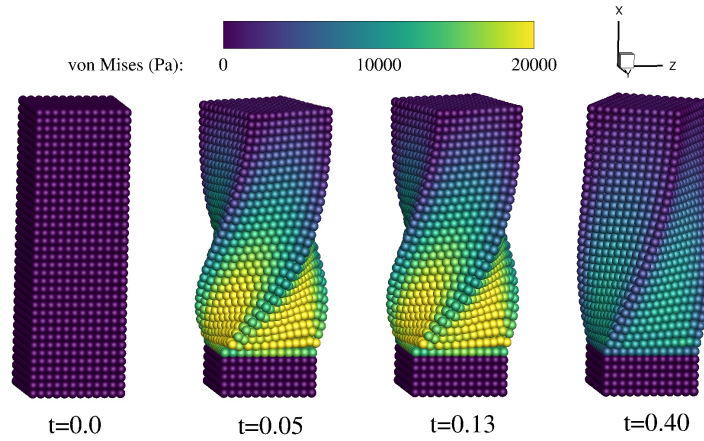


**Figure 7:** Twisting cantilever: Four time instants as labeled by blue dots in Figure 8 of deformation and von Mises stress.

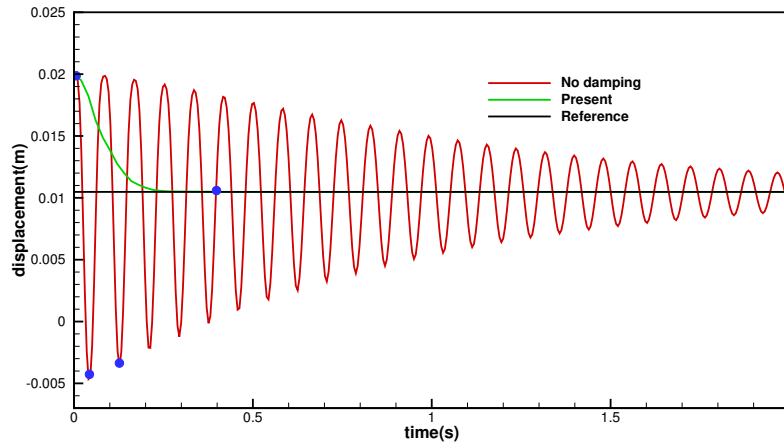


**Figure 8:** Twisting cantilever: The time history of displacement at the end point  $S$  in  $z$ - direction.

pation of the scheme. However, with the help of the present viscous damping method, the system achieves steady state faster and only few collisions is exhibited. Term "Reference" in Figure 11 denotes the final displacement ob-

tained by the conventional TLSPH method and it is clear that the present method achieves the same final results with that of the classic method.

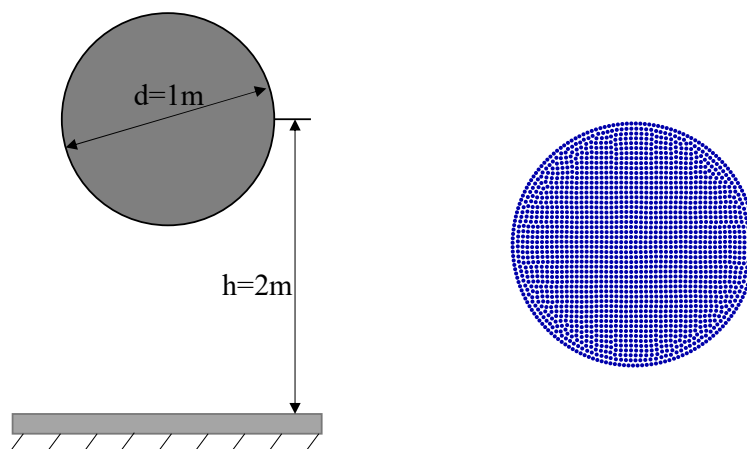


**Figure 9:** Ball free falling: Initial configuration (left panel) and body-fitted particle distribution of the ball (right panel).

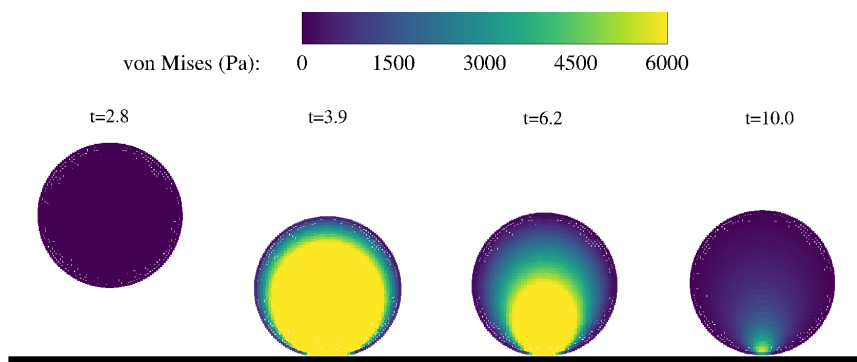


**Figure 10:** Ball free falling: Four time instants as labeled by blue dots in Figure 11 of the ball deformation and von Mises stress.



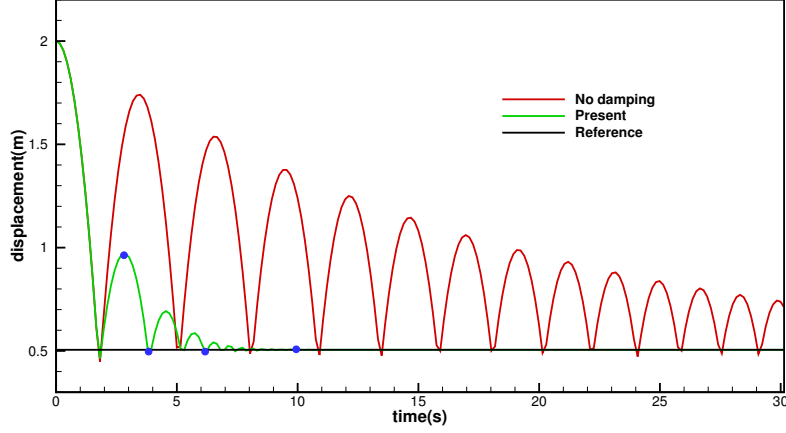


**Figure 11:** Ball free falling: The time history of the displacement at ball center in vertical direction.

#### 4.4. Hydrostatic water column on an elastic plate

This case is taken from Ref.[14] and relates to the deformation of an elastic plate induced by the hydrostatic pressure of a water column. The geometric parameters and basic setups are given in Figure 12. An aluminium plate with thick  $bh = 0.05m$  is suddenly exposed to the hydrostatic pressure loading by a  $2m$  height water column and an equilibrium state can be reached after initial oscillations. Following Refs. [14, 50, 51], the material with density of  $\rho = 2700kg/m^3$ , Young's modulus  $E = 67.5GPa$  and Poisson's ratio 0.34 is applied for the aluminium plate. As for the water, the density is  $\rho = 1000kg/m^3$  and the weakly-compressible model is adopted with the sound speed of  $c = 10U_{max}$ , where  $U_{max} = 2\sqrt{gH} = 8.86m/s$  is the maximum anticipated flow speed. In fluid-structure coupling, multiple time steps are applied. Similar to Refs. [14, 50, 51], a constant fluid time-step size  $\Delta t^F = 2.0 \times 10^{-5}s$  is adopted. More details of fluid structure interaction formulation

with SPH method are referred to Ref. [14]. In this case, the viscous damping is also introduced to water part and the corresponding artificial dynamic viscosity is given by  $\eta_f = \rho U_{max} L_f = 8858.9 kg/(m \cdot s)$  with  $L_f$  denoting the characteristic length. According to theoretical solution, the magnitude of the static deformation at the mid-span of the plate is  $d = -6.85 \times 10^{-5} m$ .

The time history of mid-span displacement for spatial resolution  $bh/dp = 4$  is presented in the top panel of Figure 13. Term "Present-plate" denotes the viscous damping only imposed on the elastic plate, "Present-fluid" is the solution with viscous damping introduced to water part and "Exact" represents the theoretical solution. It can be observed that the solution with plate damping is similar to that of without artificial damping imposed and oscillations are not repressed effectively. In fact, the oscillation of the plate is mainly induced by the water. When the present viscous damping is introduced to water, the solution reaches the equilibrium state rapidly as shown in Figure 13. Moreover, a convergence study with the present viscous damping imposed on water part is carried out by increasing the spatial resolution. The results are given in bottom panel of Figure13 and it is clear that a convergent displacement of the mid-span is achieved implying the accuracy of the present method.

The CPU wall-clock time of the viscous damping process is recorded in Table 2 until the physical time of  $t = 2s$ . It can be observed that the damping process only takes 26.89s during the computing and almost 5 times speedup is achieved by implementing share-memory parallelization. Besides, if an explicit scheme instead of the present implicit schemes is implemented for viscous damping, the fluid time-step size would be limited to  $\Delta t^F \leq$

**Table 2:** CPU time for viscous damping process in the simulation of hydrostatic water column on an elastic plate.

	serial computation	parallel computation
CPU time (s)	133.57	26.89

$0.25 \frac{h^2}{\nu} = 4.4 \times 10^{-6} s$  according to Eq.(21), which is much smaller than the adopted constant fluid time-step size  $\Delta t^F = 2.0 \times 10^{-5} s$  demonstrating the efficiency of the present method.

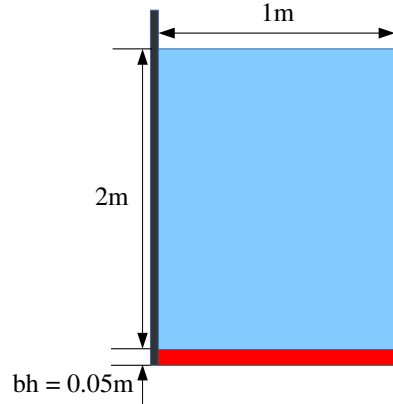


**Figure 12:** Hydrostatic water column on an elastic plate: Initial configuration.

## 5. Conclusions

In this paper, an efficient dynamic relaxation method for SPH method is proposed by imposing viscous damping to a dynamic system. This method mainly includes the following aspects: (a) a viscous damping term is added to the momentum conservation equation and two operator splitting schemes are introduced to discretize this term; (b) a random-choice strategy is introduced to release the system from large damping; (c) a splitting CLL method is pro-

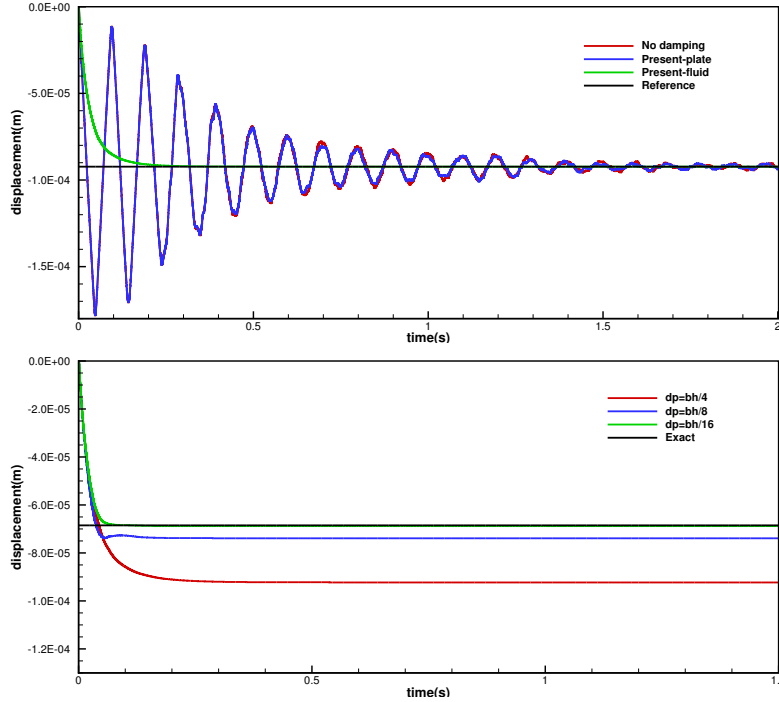


**Figure 13:** Hydrostatic water column on an elastic plate: Mid-span displacement at resolution of  $dp = bh/4$  (top panel) and a convergence study with increasing spatial resolutions (bottom panel).

posed to address the conflicts between different threads in shared-memory parallelization. The implicit nature of the splitting scheme makes the discretization stable and large time-step size is allowable. The random-choice strategy helps to eliminate the path dependency, improve the convergence rate and also reduce much computational cost. A various of test cases demonstrate the improved efficiency and performance of the present method for achieving the final converged state of a system compared to conventional SPH method. Besides, the proposed splitting CLL is thread-conflict free and makes it possible for implicit methods adopting share-memory parallel

techniques to further improve computational performance. Moreover, other implicit methods, e.g. the splitting scheme [38] for highly dissipative problem and compact finite different scheme [52] for hyperbolic problems, encounter the same problem of thread-conflict in shared-memory parallelization. The present splitting CLL scheme also provides a practicable solution to these problems by dividing computational domain into several blocks, which is the subject of our ongoing work.

### **Acknowledgements**

The first author is partially supported by Xidian University (China) and the project of National Natural Science Foundation of China (NSFC) (Grant No:91952110). C. Zhang and X.Y. Hu would like to express their gratitude to Deutsche Forschungsgemeinschaft for their sponsorship of this research under grant number DFG HU1572/10-1 and DFG HU1527/12-1.

### **References**

- [1] T. Belytschko, Y. Krongauz, D. Organ, M. Fleming, P. Krysl, Meshless methods: An overview and recent developments, *Computer methods in applied mechanics and engineering* 139 (1) (1996) 3–47.
- [2] G.-R. Liu, Y.-T. Gu, *An introduction to meshfree methods and their programming*, Springer Science & Business Media, 2005.
- [3] M. Liu, G. Liu, Smoothed particle hydrodynamics (SPH): An overview and recent developments, *Archives of computational methods in engineering* 17 (1) (2010) 25–76.

- [4] L. B. Lucy, A numerical approach to the testing of the fission hypothesis, *The astronomical journal* 82 (1977) 1013–1024.
- [5] R. A. Gingold, J. J. Monaghan, Smoothed particle hydrodynamics: Theory and application to non-spherical stars, *Monthly notices of the royal astronomical society* 181 (3) (1977) 375–389.
- [6] J. J. Monaghan, Simulating free surface flows with SPH, *Journal of computational physics* 110 (2) (1994) 399–406.
- [7] X. Y. Hu, N. A. Adams, A multi-phase SPH method for macroscopic and mesoscopic flows, *Journal of Computational Physics* 213 (2) (2006) 844–861.
- [8] S. Shao, C. Ji, D. I. Graham, D. E. Reeve, P. W. James, A. J. Chadwick, Simulation of wave overtopping by an incompressible SPH model, *Coastal engineering* 53 (9) (2006) 723–735.
- [9] C. Zhang, G. Xiang, B. Wang, X. Hu, N. A. Adams, A weakly compressible SPH method with WENO reconstruction, *Journal of Computational Physics* 392 (2019) 1–18.
- [10] W. Benz, E. Asphaug, Simulations of brittle solids using smooth particle hydrodynamics, *Computer physics communications* 87 (1-2) (1995) 253–265.
- [11] P. Randles, L. D. Libersky, Smoothed particle hydrodynamics: Some recent improvements and applications, *Computer methods in applied mechanics and engineering* 139 (1-4) (1996) 375–408.

- [12] J. J. Monaghan, Sph without a tensile instability, *Journal of computational physics* 159 (2) (2000) 290–311.
- [13] C. Antoci, M. Gallati, S. Sibilla, Numerical simulation of fluid–structure interaction by SPH, *Computers & structures* 85 (11-14) (2007) 879–890.
- [14] C. Zhang, M. Rezavand, X. Hu, A multi-resolution SPH method for fluid-structure interactions, *Journal of Computational Physics* (2020) 110028.
- [15] C. Zhang, J. Wang, M. Rezavand, D. Wu, X. Hu, An integrative smoothed particle hydrodynamics framework for modeling cardiac function, *arXiv preprint arXiv:2009.03759* (2020).
- [16] J. W. Swegle, D. L. Hicks, S. W. Attaway, Smoothed particle hydrodynamics stability analysis, *Journal of computational physics* 116 (1) (1995) 123–134.
- [17] J. P. Morris, *Analysis of smoothed particle hydrodynamics with applications*, Monash University Australia, 1996.
- [18] J. J. Monaghan, Smoothed particle hydrodynamics, *Annual review of astronomy and astrophysics* 30 (1) (1992) 543–574.
- [19] G. R. Johnson, Artificial viscosity effects for sph impact computations, *International Journal of Impact Engineering* 18 (5) (1996) 477–488.
- [20] J. Chen, J. Beraun, T. Carney, A corrective smoothed particle method for boundary value problems in heat conduction, *International Journal for Numerical Methods in Engineering* 46 (2) (1999) 231–252.

- [21] J. Chen, J. Beraun, A generalized smoothed particle hydrodynamics method for nonlinear dynamic problems, *Computer Methods in Applied Mechanics and Engineering* 190 (1-2) (2000) 225–239.
- [22] J. Bonet, S. Kulasegaram, A simplified approach to enhance the performance of smooth particle hydrodynamics methods, *Applied Mathematics and Computation* 126 (2-3) (2002) 133–155.
- [23] M. B. Liu, W. Xie, G. Liu, Modeling incompressible flows using a finite particle method, *Applied mathematical modelling* 29 (12) (2005) 1252–1270.
- [24] M. Liu, G.-R. Liu, Restoring particle consistency in smoothed particle hydrodynamics, *Applied numerical mathematics* 56 (1) (2006) 19–36.
- [25] C. Dyka, R. Ingel, An approach for tension instability in smoothed particle hydrodynamics (SPH), *Computers & structures* 57 (4) (1995) 573–580.
- [26] C. Dyka, P. Randles, R. Ingel, Stress points for tension instability in SPH, *International Journal for Numerical Methods in Engineering* 40 (13) (1997) 2325–2341.
- [27] P. Randles, L. Libersky, Normalized SPH with stress points, *International Journal for Numerical Methods in Engineering* 48 (10) (2000) 1445–1462.
- [28] J. J. Monaghan, Smoothed particle hydrodynamics and its diverse applications, *Annual Review of Fluid Mechanics* 44 (2012) 323–346.



- [29] T. Ye, D. Pan, C. Huang, M. Liu, Smoothed particle hydrodynamics (SPH) for complex fluid flows: Recent developments in methodology and applications, *Physics of Fluids* 31 (1) (2019) 011301.
- [30] J. R. H. Otter, A. C. Cassell, R. E. Hobbs, POISSON, Dynamic relaxation, *Proceedings of the Institution of Civil Engineers* 35 (4) (1966) 633–656.
- [31] T. Belytschko, W. K. Liu, B. Moran, K. Elkhodary, *Nonlinear finite elements for continua and structures*, John wiley & sons, 2013.
- [32] S. Jung, T.-Y. Kim, W.-S. Yoo, Dynamic relaxation using continuous kinetic damping—part i: Basic algorithm, *Journal of Computational and Nonlinear Dynamics* 13 (8) (2018).
- [33] J. Rodriguez, Numerical study of dynamic relaxation methods and contribution to the modelling of inflatable lifejackets, Ph.D. thesis, Ph. D. thesis, Université de Bretagne Sud (2011).
- [34] J. Alamatian, A new formulation for fictitious mass of the dynamic relaxation method with kinetic damping, *Computers & Structures* 90 (2012) 42–54.
- [35] M. Rezaiee-Pajand, H. Rezaee, Fictitious time step for the kinetic dynamic relaxation method, *Mechanics of Advanced Materials and Structures* 21 (8) (2014) 631–644.
- [36] J. Lin, H. Naceur, D. Coutellier, A. Laksimi, Efficient meshless SPH method for the numerical modeling of thick shell structures undergoing

- large deformations, *International Journal of Non-Linear Mechanics* 65 (2014) 1–13.
- [37] I. Zardi, J. Alamatian, A new formulation for fictitious mass of viscous dynamic relaxation method, *Mechanics Based Design of Structures and Machines* 48 (5) (2020) 542–567.
- [38] S. Litvinov, M. Ellero, X. Hu, N. A. Adams, A splitting scheme for highly dissipative smoothed particle dynamics, *Journal of Computational Physics* 229 (15) (2010) 5457–5464.
- [39] G. Contreras, M. Martonosi, Characterizing and improving the performance of intel threading building blocks, in: *2008 IEEE International Symposium on Workload Characterization*, IEEE, 2008, pp. 57–66.
- [40] C. Zhang, M. Rezavand, Y. Zhu, Y. Yu, D. Wu, W. Zhang, S. Zhang, J. Wang, X. Hu, SPHinXsys: An open-source meshless, multi-resolution and multi-physics library, *Software Impacts* 6 (2020) 100033.
- [41] R. Vignjevic, J. R. Reveles, J. Campbell, SPH in a total lagrangian formalism, *CMC-Tech Science Press*- 4 (3) (2006) 181.
- [42] J.-H. Wang, S. Pan, X. Y. Hu, N. A. Adams, A split random time-stepping method for stiff and nonstiff detonation capturing, *Combustion and Flame* 204 (2019) 397–413.
- [43] R. I. McLachlan, G. R. W. Quispel, Splitting methods, *Acta Numerica* 11 (2002) 341.

- [44] G. Strang, On the construction and comparison of difference schemes, *SIAM journal on numerical analysis* 5 (3) (1968) 506–517.
- [45] K. Nguyen, A. Caboussat, D. Dabdub, Mass conservative, positive definite integrator for atmospheric chemical dynamics, *Atmospheric Environment* 43 (40) (2009) 6287–6295.
- [46] M. A. Nielsen, *Neural networks and deep learning*, Vol. 25, Determination press USA, 2015.
- [47] M. Crisfield, *Non-linear finite element analysis of solids and structures: Advanced topics* (1997).
- [48] G.-R. Liu, M. B. Liu, *Smoothed particle hydrodynamics: A meshfree particle method*, World scientific, 2003.
- [49] H. Wendland, Piecewise polynomial, positive definite and compactly supported radial functions of minimal degree, *Advances in computational Mathematics* 4 (1) (1995) 389–396.
- [50] G. Fourey, C. Hermange, D. Le Touzé, G. Oger, An efficient FSI coupling strategy between smoothed particle hydrodynamics and finite element methods, *Computer Physics Communications* 217 (2017) 66–81.
- [51] A. Khayyer, H. Gotoh, H. Falahaty, Y. Shimizu, An enhanced ISPH–SPH coupled method for simulation of incompressible fluid–elastic structure interactions, *Computer Physics Communications* 232 (2018) 139–164.

- [52] S. K. Lele, Compact finite difference schemes with spectral-like resolution, *Journal of computational physics* 103 (1) (1992) 16–42.